Supplemental information: Preferential Adsorption in Mixed Electrolytes Confined by Charged Amorphous Silica

Max F. Döpke,[†] Johannes Lützenkirchen,[‡] Othonas A. Moultos,[†] Bertrand Siboulet,[¶] Jean-François Dufrêche,[¶] Johan T. Padding,[†] and Remco Hartkamp[*,†]

[†]*Process & Energy Department, Delft University of Technology, Leeghwaterstraat 39, 2628 CB Delft, The Netherlands*

[‡]*Institut für Nukleare Entsorgung, Karlsruher Institut für Technologie, P.O. Box 3640, 76021 Karlsruhe, Germany*

[¶]*Institut de Chimie Séparative de Marcoule ICSM, UMR 5257 CEA, CNRS, ENSCM, Université Montpellier, Bâtiment 426, F-30207 Bagnols-sur-Cèze, France*

E-mail: r.m.hartkamp@tudelft.nl

1 Supporting figures and tables

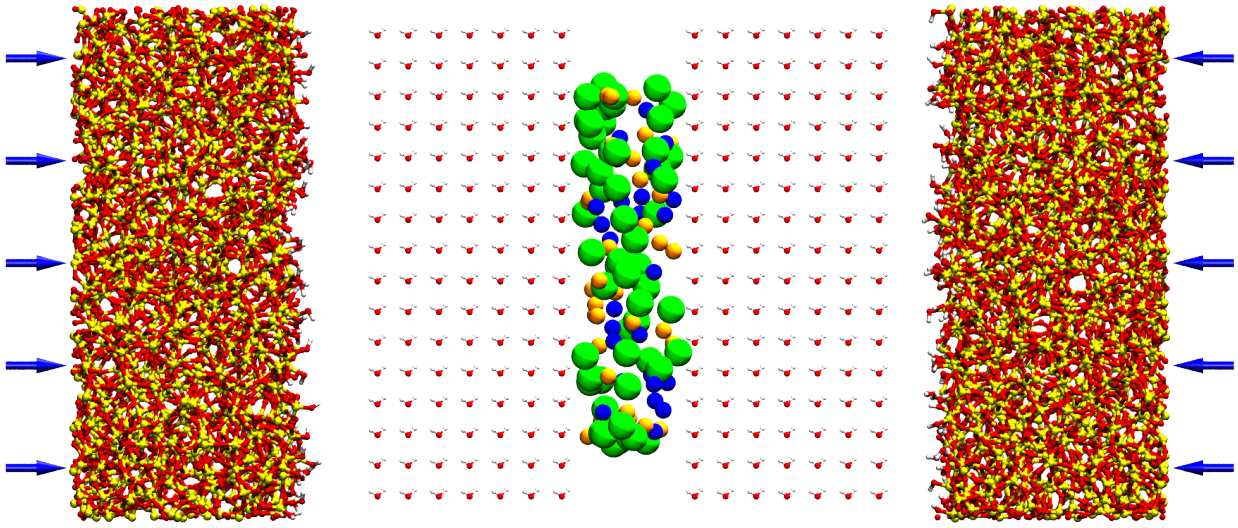

Figure S1: Initial set-up of system before compression. Arrows indicate movement of walls due to an applied force equivalent to 1 bar to adjust fluid density.

Table S1: Dangling oxygen PM, selectivity, number of adsorbed ions (if adsorbed) and coordination number of adsorbed ions. Letters I, V and G stand for Isolated, Vicinal and Geminal respectively. Left and right indicate the surface of the dangling oxygen from figures 8 and S3

Loc.	Type	PM	Specificity	Na^+	CN_{Na^+}	Ca^{2+}	$CN_{Ca^{2+}}$
left	V	1.04	0.34	1.04	3.57	1.00	5.67
left	V	1.02	-0.03	1.00	3.27	1.00	6.12
left	V	1.00	0.15	1.00	3.57	1.00	4.91
left	V	1.03	0.10	1.00	3.73	1.00	5.03
left	G	1.01	0.61	1.00	3.83	1.00	5.04
left	V	1.03	-0.55	1.00	4.01	1.00	5.19
left	I	1.03	0.52	1.00	3.85	1.00	6.14
left	V	1.04	0.53	1.12	3.96	1.00	4.65
left	V	1.03	0.48	1.01	3.62	1.00	4.00
left	I	1.04	0.05	1.11	3.23	1.00	5.57
left	V	1.04	0.73	1.29	3.63	1.00	3.80
left	V	0.99	0.00	0.00	0.00	0.00	0.00
left	G	1.03	-0.23	1.00	4.07	1.00	5.16
left	V	1.04	-0.62	1.00	4.71	1.00	5.13
left	G	1.02	-0.35	1.21	4.16	1.00	5.17
left	V	1.01	0.50	1.00	4.53	1.00	5.43
right	I	1.05	-0.52	1.00	2.95	1.00	5.04
right	V	1.08	-0.46	0.00	0.00	1.00	5.77
right	G	1.01	-0.65	1.00	3.69	1.00	4.44
right	G	1.00	-0.40	1.21	2.85	1.20	4.12
right	I	1.06	-0.25	1.00	4.27	1.00	5.43
right	G	1.03	0.18	1.00	2.89	1.00	4.31
right	I	1.03	0.03	1.00	3.22	1.00	5.10
right	V	1.01	0.00	1.00	3.31	1.00	3.83
right	G	1.02	0.55	1.83	3.38	1.00	5.06
right	I	1.04	-0.37	1.00	4.31	1.00	5.38
right	G	1.04	0.65	1.75	3.53	1.00	5.06
right	G	1.01	-0.58	1.25	3.42	1.10	4.03
right	I	1.04	0.18	1.14	2.97	1.00	4.42
right	V	1.03	-0.35	1.00	3.49	1.00	5.26
right	V	1.00	0.09	1.33	2.68	1.00	3.35
right	I	1.07	-0.33	1.00	5.46	1.00	5.45
right	I	1.56	-0.28	1.00	4.25	1.00	6.66

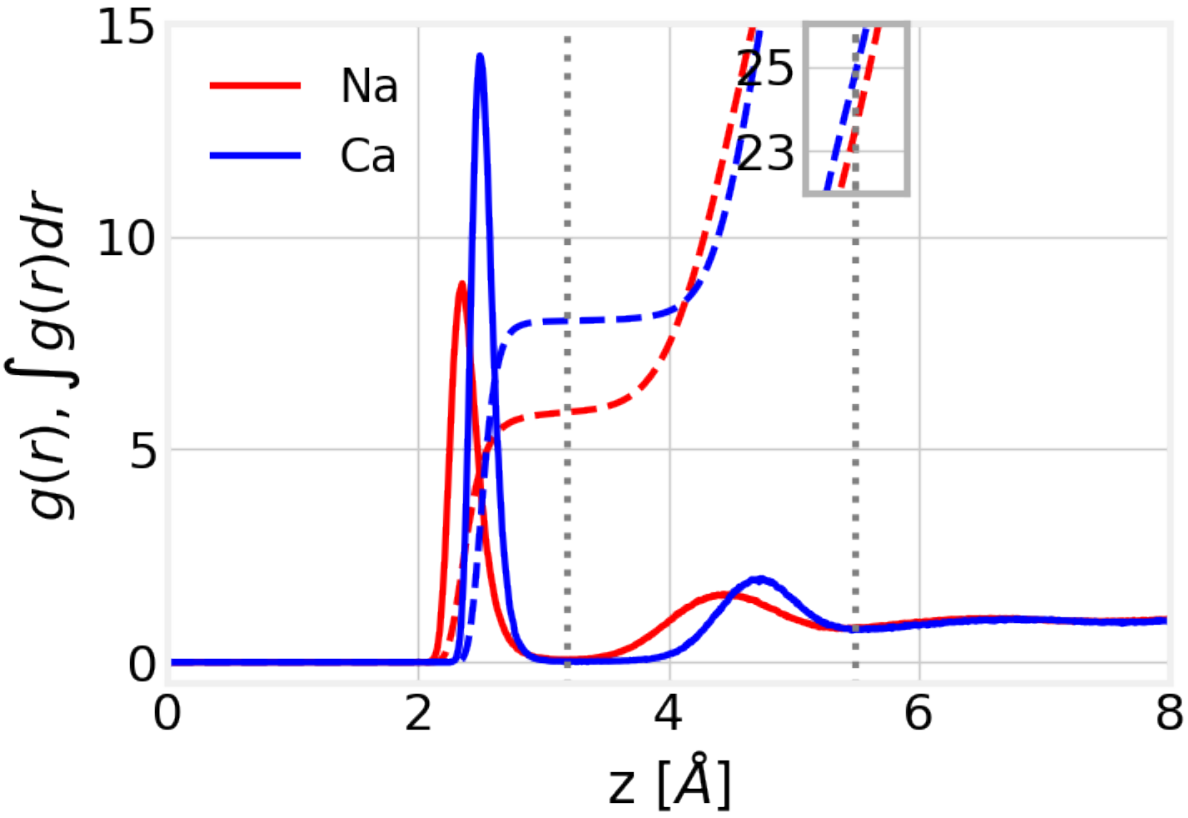

Figure S2: Rdf of ion-water for Na^{+} and Ca^{2+}

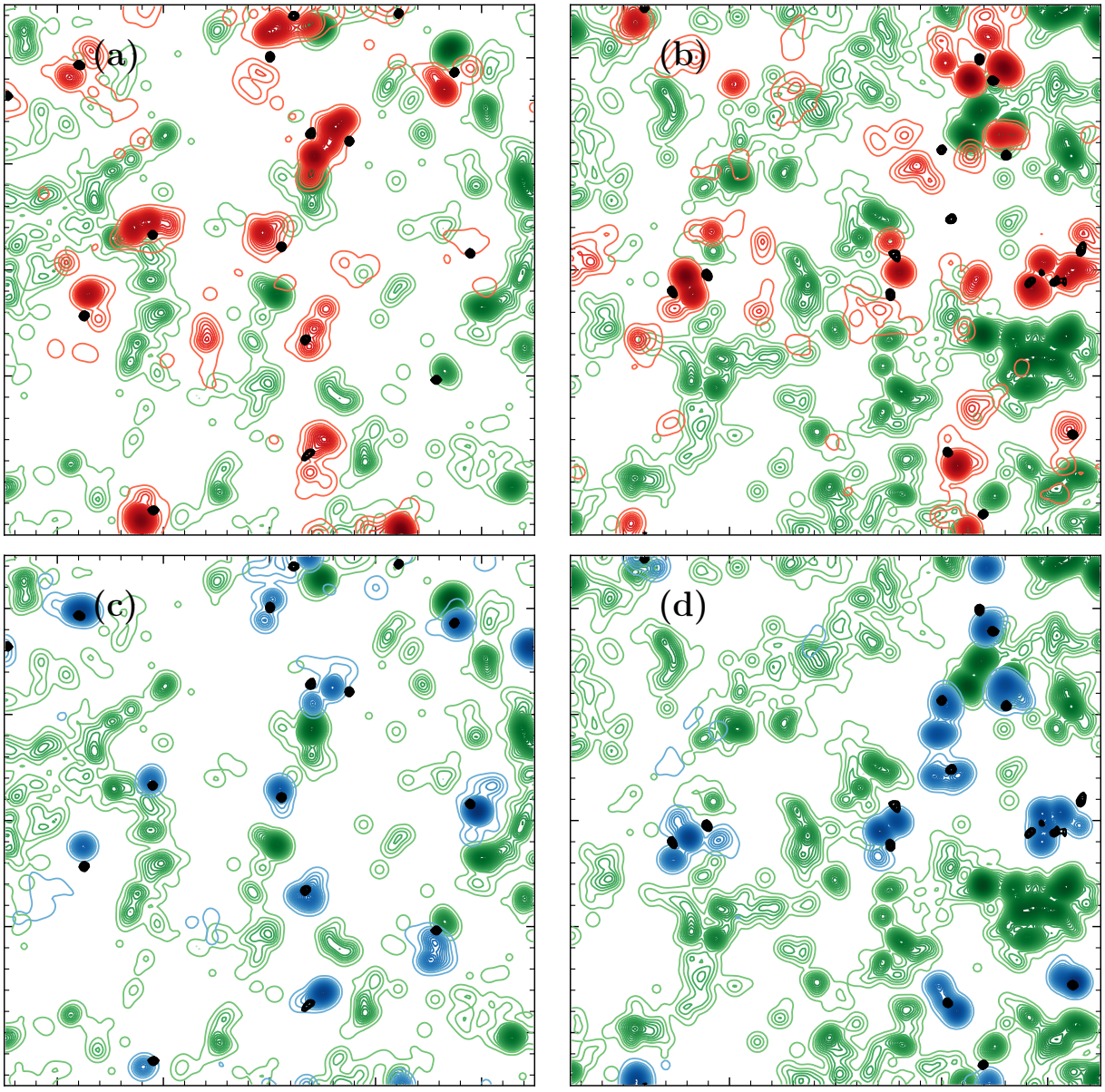

Figure S3: Average adsorption location of Na^+ (red in (a) and (b)) and Ca^{2+} (blue in (c) and (d)) on the left ((a) and (c)) and right ((b) and (d)) walls from single species 0.3Na and 0.3Ca systems. Average Cl^- adsorption location is given in green.

2 Computational details

The computations are split into two main stages: 1) obtaining a block of amorphous silica, and 2) channel simulations. For all simulations, the Lorentz-Berthelot mixing rules, given by equations S1 and S2, were used.

$$\sigma_{ij} = \frac{\sigma_{ii} + \sigma_{jj}}{2} \tag{S1}$$

$$\epsilon_{ij} = \sqrt{\epsilon_{ii}\epsilon_{jj}} \tag{S2}$$

2.1 Creation of amorphous silica

Amorphous silica was created with a modified BKS[1] potential from Geske and Vogel,[2] with an added smoothing factor ($\frac{\exp(r-r_{s,ij})}{10}$) to avoid a nonphysical jump in the potential energy profile. The proposed modification from Geske and Vogel adds a Lennard-Jones (LJ) potential, to eliminate the nonphysical attractive forces that originate from the Buckingham potential when two atoms move too close to each other. The effect of the correction is shown in figure S4. This figure shows how the attractive forces of the BKS potential are reversed to repulsive forces when adding the LJ harmonic at distances below $r_{ij} = 1.09$ for O-O interactions and $r_{ij} = 1.50$ for O-Si interactions. Force field parameters are provided in table S2.

$$E_{pot} = \sum_{ij} \begin{cases} A_{ij}\exp(-b_{ij}r_{ij}) - \frac{c_{ij}}{r^6} + \frac{1}{4\pi\varepsilon_0}\frac{q_i q_j}{r_{ij}} & \text{for } r > r_{s,ij} \\ \frac{\exp(r-r_{s,ij})}{10}\left[\frac{C_{ij}^{(12)}}{r_{ij}^{12}} - \frac{C_{ij}^{(6)}}{r_{ij}^{6}}\right] - A_{ij}\exp(-b_{ij}r_{s,ij}) + \frac{c_{ij}}{r_{s,ij}^6} - \frac{1}{4\pi\varepsilon_0}\frac{q_i q_j}{r_{s,ij}} & \text{for } r < r_{s,ij} \end{cases} \tag{S3}$$

In order to obtain amorphous silica, first the unit cell of β-cristobalite is replicated in the x, y and z-directions with a spacing of 101% of the unit cell length. This adjusts the density

Table S2: Force field parameters for the BKS force field and its modification. Partial charges are assigned as follows: $q_{\mathbf{O}} = -1$ e and $q_{\mathbf{Si}} = +2$ e.

	A_{ij} [Kcal/mol]	b_{ij} [Å]	c_{ij} [Kcal/mol Å^6]	$C_{ij}^{(12)}$ [KcalÅ^{12}/mol]	$C_{ij}^{(6)}$ [KcalÅ^6/mol]
O-O	32025.85802	2.76	175	281743	-2275.22
O-Si	415176.39808	4.87318	133.5381	13776	1127.08

of the crystal to be 2.21624 g/cc. Second the crystal is equilibrated, annealed, cooled and equilibrated again in the NVT ensemble, as described in table S3. During equilibration at 4000 K the structure is seen to become fully liquid. The cooling rate used is 2.5 K/ps, which is a compromise between accuracy and computational cost.[3]

Table S3: Simulation sequence for creation of amorphous silica with most important input parameters for MD code.

	Equilibration 1	Anealing	Equilibration 2	Quenching	Equilibration 3
ensemble	NVT	NVT	NVT	NVT	NVT
runtime [ps]	100	1000	1000	23000	1000
dt [fs]	1	1	1	1	1
Tstart [K]	298	298	4000	4000	298
Tend [K]	298	4000	4000	298	298
Tdamp [fs]	100	100	100	100	
tchain	3	3	3	3	3
drag	0	0	0	0	0
shift	yes	yes	yes	yes	yes

2.2 Channel simulations

Channel simulations were performed with a combination of force fields. The interface parametrization of Emami et al.[4] was used for silica, TIP4P/2005[5] for water, and ion parameters were obtained from Joung and Cheatham[6] for Na^+ and Cl^-, and Mamatkulov et al.[7] for Ca^{2+}. Table S4 provides an overview of force field parameters. The potential energy is described by equation S4.

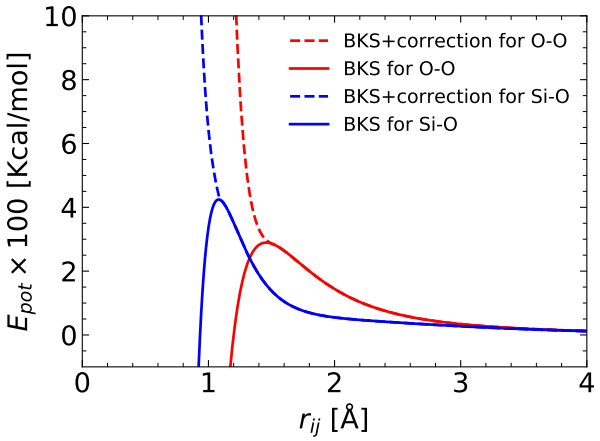

Figure S4: Potential energy of the BKS potential with and without LJ correction.

$$
\begin{aligned}
E_{pot} = & \sum_{ij,\text{nonbonded 1-2,1-4 incl and 1-3 exl}} \varepsilon_{ij} \left[\left(\frac{\sigma_{ij}}{r_{ij}} \right)^{12} - 2 \left(\frac{\sigma_{ij}}{r_{ij}} \right)^{6} \right] \\
& + \frac{1}{4\pi\varepsilon_0} \sum_{ij,\text{nonbonded 1-2,1-4 incl and 1-3 exl}} \frac{q_i q_j}{r_{ij}} \\
& + \sum_{ij,\text{bonded}} k_{r,ij} \left(r_{ij} - r_{0,ij} \right)^2 + \sum_{ijk,\text{bonded}} k_{r,ijk} \left(\theta_{ijk} - \theta_{0,ijk} \right)^2
\end{aligned}
\tag{S4}
$$

3 Amorphous silica characterization

Following the creation of amorphous silica as specified above, the final structure was analyzed and compared to known experimental and previous MD results. A comparison for the rdf peaks is provided in table S5. Furthermore, over- and undercoordinated structures are shown to be below 0.2% in table S6.

$$
g(r) = \frac{1}{\frac{N_i}{V_{\text{box}}} N_j} \left\langle \sum_{i=1}^{N} \sum_{j \neq i}^{N} \delta \left(r - |r_i - r_j| \right) \right\rangle \tag{S5}
$$

Table S4: Force field parameters for channel simulations. Subscripts are as follows: w-water, b-bulk, d-dangling, dd-dangling dangling, s-silanol, ss-silanol silanol.

Ions	σ [Å]	ϵ/k_B [K]	q [e]
Na^{+} [6]	2.1845	84.7616	+1
Ca^{+} [7]	2.8331	140.6332	+2
Cl^{-} [6]	4.9178	5.8683	-1
TIP4P/2005 [5]	σ [Å]	ϵ/k_B [K]	q [e]
O	3.1589	93.19685	
H			+0.5564
M			-1.1128
Interface [4]	σ [Å]	ϵ/k_B [K]	q [e]
Sib	3.70	46.799	+1.1
Sid	3.70	46.799	+0.725
Sidd	3.70	46.799	+0.35*
Sis	3.70	46.799	+1.1
Siss	3.70	46.799	+1.1
Ob	3.09	27.174	-0.55
Od	3.09	61.392	-0.9
Os	3.09	61.392	-0.675
H			+0.4
* partial charge was adjusted from original force field to support doubly deprotonated geminals.			
IFF bonds [4]	k_r [Kcal/(mol Å^2)]		$r_{0,ij}$ [Å]
Si-O	285		1.68
IFF angles [4]	k_θ [Kcal/(mol rad^2)]		θ_0 [°]
O-Si-O	100		109.5
Si-O-Si	100		149.0
Si-O-H	50		115.0

Table S5: Location of first and second peaks in rdf for amorphous silica. Rdfs for own simulations following equation S5 are given in figure S5.

	Simulation [Å]	Vollmayr et al. [3] [Å]	Experiments [Å]	
Si-O	1.61	1.595	1.608[b]	1.620[a]
	6.10	4.12		4.15
O-O	2.6	2.59	2.626[b]	2.65[a]
	5.02	5.01		4.95
Si-Si	3.14	3.16	3.077[c]	3.12[a]
	5.09	5.05		5.18

[a] Ref. [8]
[b] Ref. [9]
[c] Ref. [10]

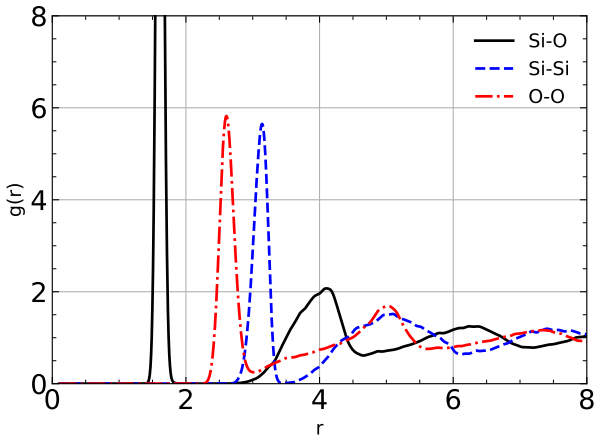

Figure S5: RDF for O-O, O-Si and Si-Si for amorphous silica obtained in this study.

Table S6: Occurrence of structures in our amorphous silica.

Structures	% occurrence
SiO_3	00.11
SiO_4	99.85
SiO_5	00.04
OSi_1	00.11
OSi_2	99.82
OSi_3	00.07

4 Uncertainty quantification

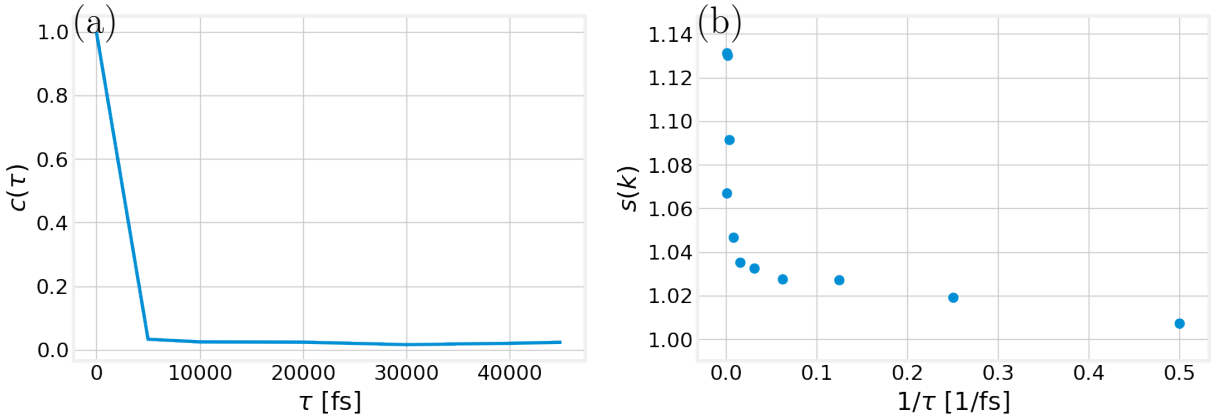

Figure S6: Correlation function of water (a) and inefficiency factor from block averaging of water (b).

For each individual simulation, the standard error was evaluated ensuring each sample was uncorrelated to the former sample. The correlation of water between frames was studied following the approach described by Allen and Tildesley.[11] The correlation function

$$c(\tau) = \frac{\langle \delta A \delta B \rangle}{\sigma_A \sigma_B} \tag{S6}$$

with

$$\delta X = X - \langle X \rangle \tag{S7}$$

and

$$\sigma_X = \langle X^2 \rangle - \langle X \rangle^2 \tag{S8}$$

was evaluated and block averaging was used yielding the same conclusion of uncorrelated results as shown in figure S6. The correlation function drops to nearly zero at the immediate next recorded time step showing no correlation and when using block averaging reducing the size of the blocks does not increase the statistical inefficiency $s(k)$ significantly above 1. Hence each sample was considered as fully independent. The standard error for each

individual simulation was defined as:

$$\mathrm{SE}_{individual} = \frac{\sigma_{individual}}{\sqrt{N_{frames}}}, \tag{S9}$$

with

$$\sigma^2_{individual} = E(x^2) - E(x)^2. \tag{S10}$$

The error SE_{multi} between simulations and from symmetrizing was computed following

$$\mathrm{SE}_{multi} = \frac{\sigma_{multi}}{\sqrt{N_{simulations}}} = \sqrt{\frac{1}{N_{simulations}} \sum_{X=1}^{N_{simulations}} (\mu_X - \mu)^2} \tag{S11}$$

where μ_X represents the ensemble averages of each simulation and μ the average between simulations. The final uncertainty was obtained from the addition of equations S9 and S11.

4.1 Screening function

The uncertainty quantification for the screening function was carried out with the assumptions $\Gamma(\chi = 0) = \sigma_0$ and $\Gamma(\chi = \infty) = 0$. Consequently, equation 1 in the main article was integrated from both directions to avoid cumulative additions of SE. This procedure is highlighted by the following equation:

$$\mathrm{SE}_{\Gamma}(\chi) = \frac{\int_{\min(\chi)}^{\chi} \sum_i SE_{\rho_{n,i}}(\chi') z_i d\chi' + \int_{\chi}^{\min(\chi)} \sum_i SE_{\rho_{n,i}}(\chi') z_i d\chi'}{2}. \tag{S12}$$

5 Symmetrizing results

The density profiles ρ_n vs z are symmetrized with respect to the centre of the channel and shifted by the average location of surface Oxygen atoms. Density profiles ρ_n vs d do not require symmetrizing. The effect of symmetrization is shown in figure S7, where the new

mean is given by

$$\rho_n = \frac{1}{2}(\rho_n(z<0) + \rho_n(z>0)) \tag{S13}$$

and the uncertainty is obtained from

$$\mathrm{SE}_{\rho_n} = \frac{1}{\sqrt{2}}\sqrt{\frac{1}{2}\left[(\rho_n(z<0) - \mu_{\rho_n}) + (\rho_n(z>0) - \mu_{\rho_n})\right]} + SE_{\rho_n(z<0)} + SE_{\rho_n(z>0)}. \tag{S14}$$

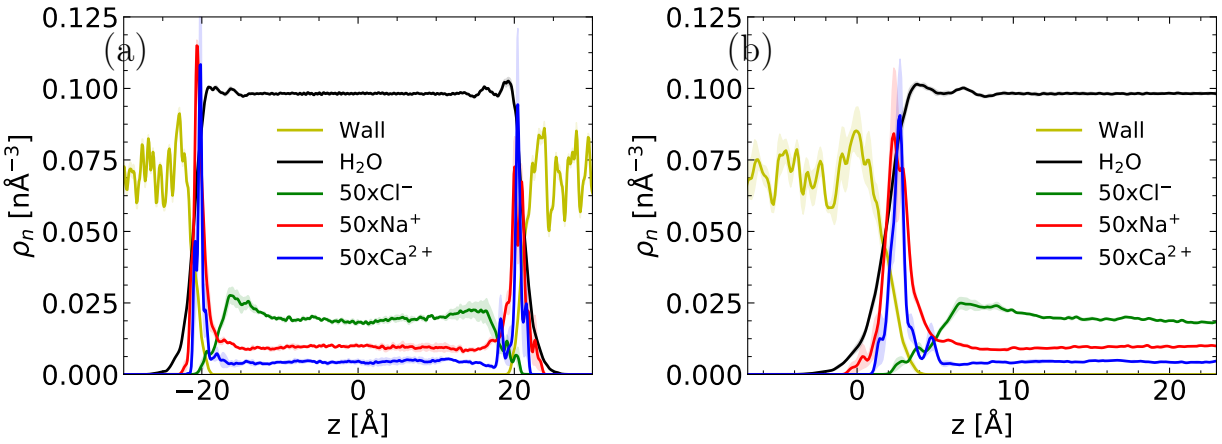

Figure S7: Unsymmetrized and symmetrized density profiles.

6 Additional density profiles

Density profiles of electrolyte compositions not provided in paper, but used in discussion are provided in figure S8.

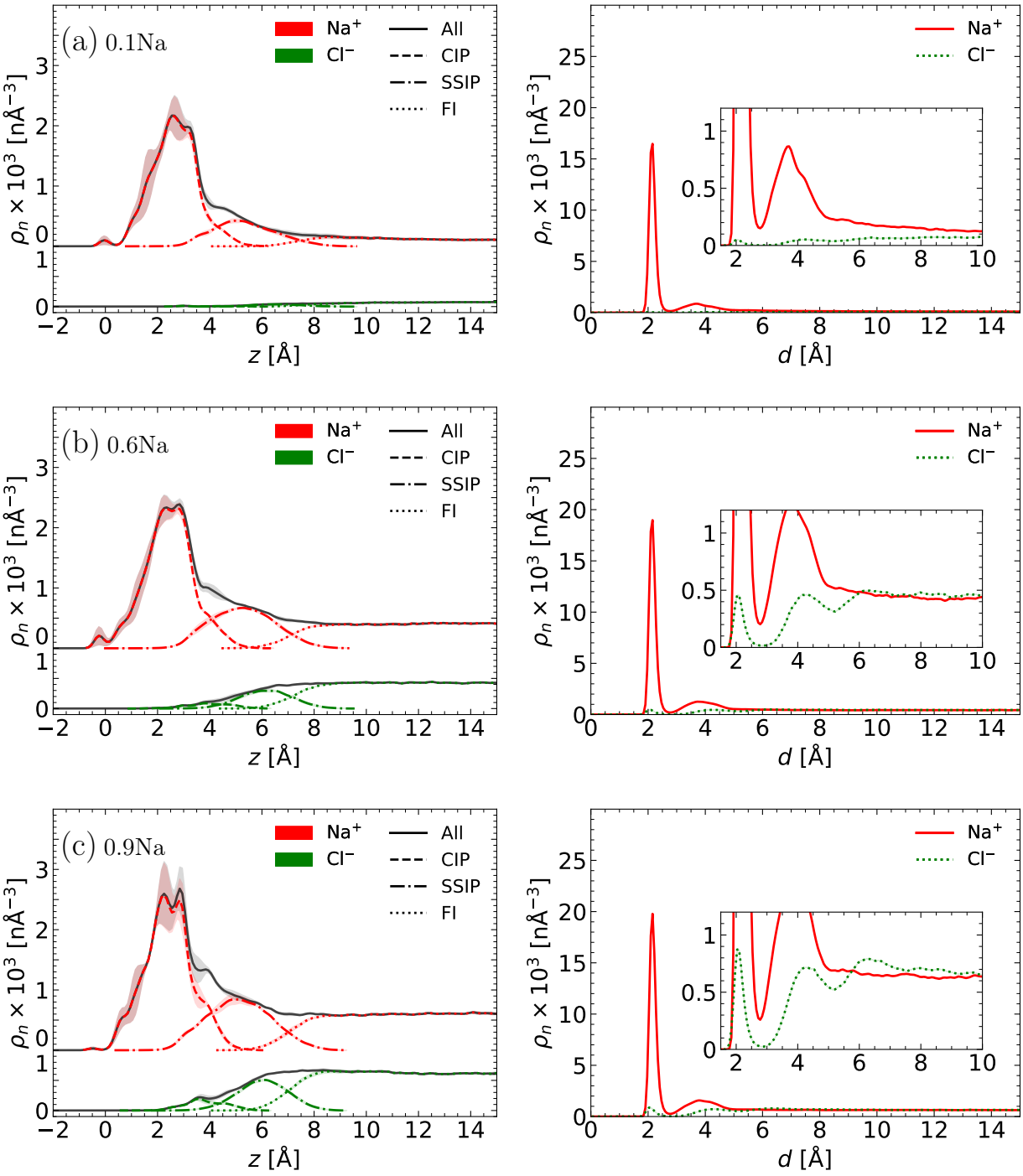
(a) 0.1Na
(b) 0.6Na
(c) 0.9Na
Na+
Cl−
All
CIP
SSIP
FI
ρn × 10³ [nÅ⁻³]
z [Å]
d [Å]

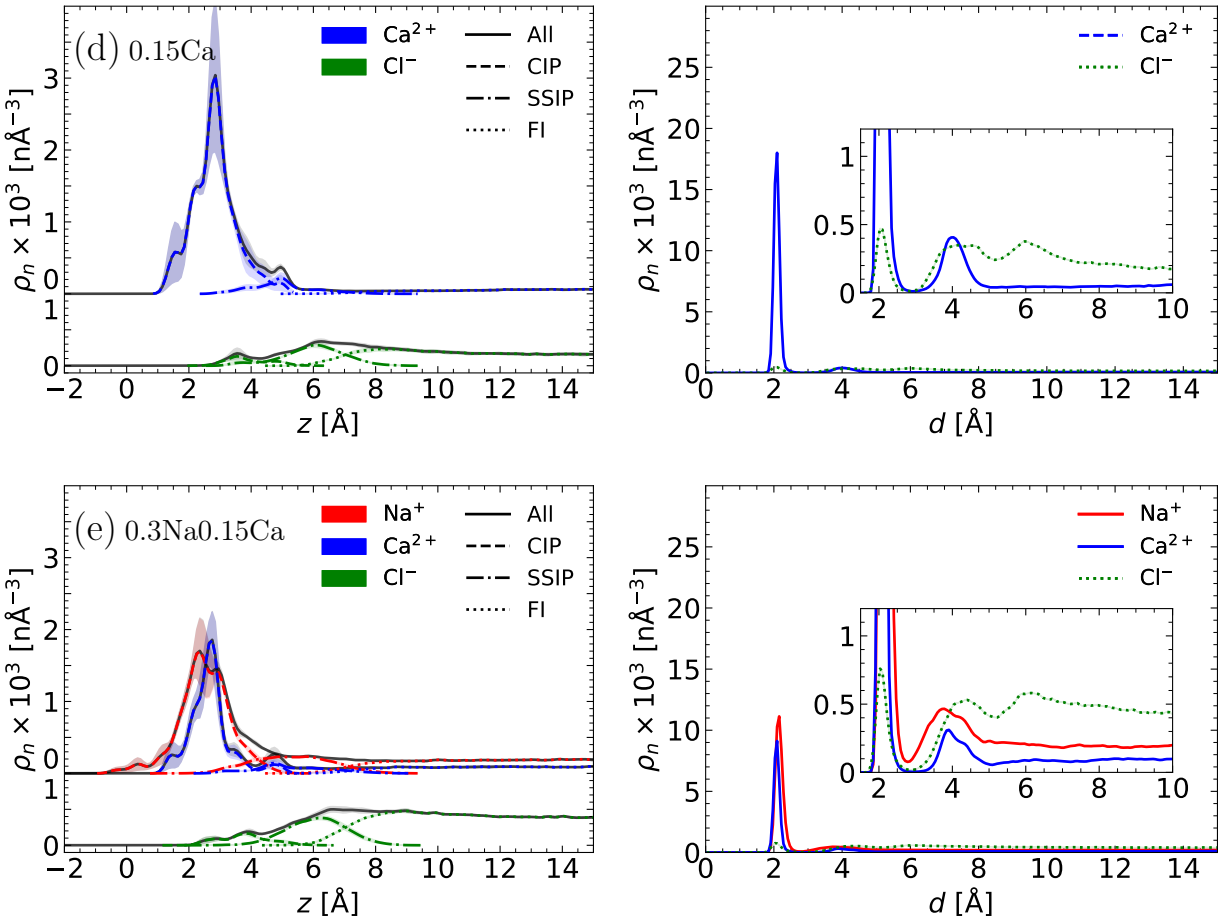

Figure S8: Density profiles for compositions not shown in the main paper. (a) 0.1Na, (b) 0.6Na, (c) 0.9Na, (d) 0.15Ca, (e) 0.3Na0.15Ca.

References

(1) Van Beest, B. W. H.; Kramer, G. J.; Van Santen, R. A. Force Fields for Silicas and Aluminophosphates Based on Ab Initio Calculations. *Phys. Rev. Lett.* **1990**, *64*, 1955–1958.

(2) Geske, J.; Vogel, M. Creating Realistic Silica Nanopores for Molecular Dynamics Simulations. *Mol. Simul.* **2017**, *43*, 13–18.

(3) Vollmayr, K.; Kob, W.; Binder, K. Cooling-Rate Effects in Amorphous Silica: A Computer-Simulation Study. *Phys. Rev. B - Condens. Matter Mater. Phys.* **1996**, *54*, 15808–15827.

(4) Emami, F. S.; Puddu, V.; Berry, R. J.; Varshney, V.; Patwardhan, S. V.; Perry, C. C.; Heinz, H. Force Field and a Surface Model Database for Silica to Simulate Interfacial Properties in Atomic Resolution. *Chem. Mater.* **2014**, *26*, 2647–2658.

(5) Abascal, J. L.; Vega, C. A General Purpose Model for the Condensed Phases of Water: TIP4P/2005. *J. Chem. Phys.* **2005**, *123*, 234505.

(6) Joung, I. S.; Cheatham, T. E. Determination of Alkali and Halide Monovalent Ion Parameters for Use in Explicitly Solvated Biomolecular Simulations. *J. Phys. Chem. B* **2008**, *112*, 9020–9041.

(7) Mamatkulov, S.; Fyta, M.; Netz, R. R. Force Fields for Divalent Cations Based on Single-Ion and Ion-Pair Properties. *J. Chem. Phys.* **2013**, *138*, 024505.

(8) Mozzi, R. L.; Warren, B. E. The Structure of Vitreous Silica. *J. Appl. Crystallogr.* **1969**, *2*, 164–172.

(9) Grimley, D. I.; Wright, A. C.; Sinclair, R. N. Neutron Scattering from Vitreous Silica IV. Time-of-Flight Diffraction. *J. Non. Cryst. Solids* **1990**, *119*, 49–64.

(10) Konnert, J. H.; Karle, J. The Computation of Radial Distribution Functions for Glassy Materials. *Acta Crystallogr. Sect. A* **1973**, *29*, 702–710.

(11) Allen, M. P.; Tildesley, D. J. *Computer Simulation of Liquids*; Oxford University Press: New York, NY, USA, 2017; Vol. 1.